# A new enrichment space for the treatment of discontinuous pressures in multi-fluid flows

**Article** *in* International Journal for Numerical Methods in Fluids · November 2012

DOI: 10.1002/fld.2713



**3 authors:**

Roberto F. Ausas
University of São Paulo
**27** PUBLICATIONS **343** CITATIONS
SEE PROFILE

Gustavo Buscaglia
University of São Paulo
**123** PUBLICATIONS **1,658** CITATIONS
SEE PROFILE

Sergio Rodolfo Idelsohn
Catalan Institution for Research and Advance…
**394** PUBLICATIONS **5,003** CITATIONS
SEE PROFILE

INTERNATIONAL JOURNAL FOR NUMERICAL METHODS IN FLUIDS
*Int. J. Numer. Meth. Fluids* 2011; **00**:1–23
Published online in Wiley InterScience (www.interscience.wiley.com). DOI: 10.1002/fld

# A new enrichment space for the treatment of discontinuous pressures in multi–fluid flows

Roberto F. Ausas[1], Gustavo C. Buscaglia[1] and Sergio R. Idelsohn[2*]

[1]*Instituto de Ciências Matemáticas e Computação, Universidade de São Paulo, Av. do Trabalhador Sãocarlense 400, 13560-970 São Carlos, SP, Brazil*
[2]*ICREA Research Professor, Centro Internacional de Métodos Numéricos en Ingeniería., Edificio C1, Campus Norte UPC C/ Gran Capitán S/N 08034 Barcelona, España*

SUMMARY

In this work, a new enrichment space to accomodate jumps in the pressure field at immersed interfaces in finite element formulations, is proposed. The new enrichment adds two degrees of freedom per element that can be eliminated by means of static condensation. The new space is tested and compared to other existing finite element space and with the classical $P_1$ space in several problems involving jumps in the viscosity and/or the presence of singular forces at interfaces not conforming with the element edges. The combination of this enrichment space with an additional enrichment to accomodate discontinuities in the pressure gradient has also been explored, exhibiting excelent results in problems involving jumps in the density or the volume forces. Copyright © 2011 John Wiley & Sons, Ltd.

Received . . .

KEY WORDS: Multi–fluids, Two–phase flows, Embedded interfaces, Finite element method, Surface tension, discontinuous pressures, kinks.

## 1. INTRODUCTION

The simultaneous presence of multiple fluids with varying properties in external or internal flows is found in daily life, marine environmental problems, and numerous industrial processes, among many other practical situations. Examples of these flows are gas–liquid transport, magma chambers, fluid–fuel interactions, crude oil recovery, spray cans, sediment transport in rivers and floods, pollutant transport in the atmosphere, cloud formation, fuel injection in engines, bubble column reactors and spray dryers for food processing, among others. This shows the importance of multi–fluid flows, which probably occur even more frequently than single phase flows [1]. As a result of the interaction between the different fluid components, multi–fluid flows are rather complex and very difficult to describe theoretically. For homogeneous flows, computational of fluid dynamics (CFD) has already a long history and it is standard practice to use commercially available CFD codes. However, because of the complex physics involved in multi–fluid flows the application of CFD in this area is rather young. Physical modeling in ad–hoc laboratory scale models is not suitable for this purpose because of its complexity, the difficulty for scaling up to real life problems and hence unaffordable costs. The alternative is therefore numerical modeling.

Despite the practical importance of the problem and the intensive work carried out in the last decade for the development of suitable mathematical and computational models, it is widely accepted that the numerical study of heterogeneous flows is still a major challenge [1]. The

*Correspondence to: Centro Internacional de Métodos Numéricos en Ingeniería., Edificio C1, Campus Norte UPC C/ Gran Capitán S/N 08034 Barcelona, España

complicated mathematical structure of the multi–fluid problem, the multi–scale features of the flow, the existence of one or multiple internal interfaces and the unsteadiness of the flow, constitute major challenges for the analysis.

Computing the interface between various immiscible fluids or the free–surfaces is difficult because neither the shape nor the positions of the interfaces are known a priori. The two approaches to solve these problems are: interface–tracking and interface–capturing methods. The former computes the motion of the flow particles via a Lagrangian approach where the computational domain adapts itself to the shape and position of the interfaces (see e.g. [2, 3, 4, 5, 6, 7]). A different approach for the simulation of free–surface flows that is based on Lagrangian particles can be found in [8, 9]. On the other hand, in the front–tracking method (see [10, 11, 12]), the interface is represented by a surface mesh advected with a Lagrangian method while immersed in an Eulerian (fix) mesh where the flow problem is solved considering the fluids as a single effective fluid with variable properties.

The other alternative are the interface–capturing methods. Popular methods of this type are the Volume–of–fluid technique (see [13, 14, 15]) and the level set method (see for example [16, 17, 18, 19]). In this case, the flow problem is also solved in a fixed underlying mesh considering a single fluid with variable properties. Variants of these methods mainly differ in two aspects: first, the tecnhique used to solve the transport equation for the scalar function where the interface is embedded, for which a great deal of work has been done to improve accuracy as shown for instance in [20, 21, 22, 23, 24, 25] for purely Eulerian methods and [26, 27, 28] for semi–Lagrangian methods. The other differences appear in the technique used to solve the Navier-Stokes equations for a one phase flow with variable properties and in how the fluid–dynamical variables are treated near the interface, since, these can exhibit discontinuities in their values and/or their gradients due to the discontinuities in the physical properties and/or the presence of singular forces.

Several remedies have been proposed to improve accuracy and robustness of computations in Eulerian formulations. For instance, in Brackbill et al [29] a treatment of the singular forces at the interface by means of a regularization is proposed, such that, sharp variations in the pressure field are avoided. In Löhner et al [30] and Carrica at al [31], different extrapolation techniques of the velocity and pressure near the interface are presented.

In this work, on the other hand, we focus the attention on how to improve the accuracy of simulations in finite element formulations by means of improving the approximation spaces. In this case, since a partition of the computational domain into simplices is made and the interface does not necessarily conform with the element edges, standard finite element methods, either continuous or discontinuous across inter–element boundaries, suffer from suboptimal approximation orders. This poor approximation leads to spurious velocities near the interface that may significantly affect precision and robustness of numerical simulations (see e.g. [32]). One possibility is to locally modify the finite element spaces in those elements cut by the interface in order to accomodate the discontinuities. This can be done without introducing additional degrees of freedom as shown by Ausas et al [33] in which a new finite element space has been introduced. The interpolation properties of this space are discussed in detail in [34], where the authors show that the interpolation order of this space is $\mathcal{O}(h^{\frac{3}{2}})$ in the $L^2(\Omega)$–norm, which represents an improvement with respect to the order $\mathcal{O}(h^{\frac{1}{2}})$ using the classical $P_1$–conforming space. When taken as pressure space, the accuracy of Navier–Stokes computations in equal–order velocity–pressure approximations is not limited, since the global accuracy is already limited by the $H^1(\Omega)$–accuracy of the velocity space, which is at most $\mathcal{O}(h)$.

The other possibility, that is explored in this article, is to add degrees of freedom or enrich the finite element spaces at the elements cut by the interface. Minev and co workers [35] use gradient velocity shape functions and discontinuous pressure shape functions also for problems involving surface tension. Also, for two–phase flow problems, Chessa and Belytschko [36] use an enrichment method called XFEM, initially developed by the second author for the modeling of cracks [37]. Both approaches lead to optimal orders of convergence, but the main drawback is that the additional degress of freedom cannot be eliminated before assembly. The connectivity of the unknowns depend on the position of the interface, therefore the mesh graph needs to be updated as the interface moves.



DOI: 10.1002/fld

Also, it has been observed that the resulting linear system becomes ill–conditioned and that the linear independence of the finite element basis deteriorates as the mesh size is reduced. This XFEM approach has also been used recently in [38, 39, 40] for two–phase flows. Another method that is related to the XFEM approach, but avoids the inclusion of additional degrees of freedom is presented by Fries at al [41], but some complexities related to the moving least square approach used have to be dealt with. Also, in [42], Codina and Coppola introduce an enrichment for the treatment of kinks in the pressure field as typically happens in problems with jumps in the density in the presence of a gravitational field. The additional degree of freedom can be statically condensed prior to assembly.

The main contribution of this paper is a new enrichment space for discontinuous pressures. Two enrichment functions are introduced at the elements crossed by the interface. The new functions are local to each element, linear on each side of the interface, discontinuous just at the interface and zero at the element nodes. The additional degrees of freedom can be condensed before assembly, avoiding the complexities asociated with the update of the mesh graph. The implementation in any existing finite element code is extremely easy in two and three spatial dimensions, since the new shape functions are based on the usual $P_1$ functions. As revelead in the numerical experiments, the interpolation properties of this new enrichment space are equal or better than those of the space presented in [33].

By way of outline, after this introduction, the governing equations and different jump conditions that arise in two–phase flows are recalled as well as the continuous and discrete variational formulations. Next, the new proposed enrichment space for discontinuous pressures is introduced with details to construct the enrichment functions. In section 4 several problems in 2D and 3D are solved. Then, a further enrichment is proposed to deal with problems involving both discontinuities and kinks in the pressure field, in which, the new enrichment space is combined with the enrichment of [42]. Finally, some conclusions are drawn.

## 2. MATHEMATICAL SETTING

We restrict our attention here to problems governed by the incompressible Navier–Stokes equations. Let us consider a domain $\Omega \subset \mathbb{R}^d$ ($d = 2$ or 3). The problem is to find a velocity field $\mathbf{u}$ and a pressure field $p$ such that

$$\rho\left(\partial_t \mathbf{u} + \mathbf{u}\cdot\nabla\mathbf{u}\right) - \nabla\cdot\left(2\,\mu\nabla^S\mathbf{u}\right) + \nabla p = \rho\,\boldsymbol{b} \quad \text{in } \Omega,\ t>0, \tag{1}$$

$$\nabla\cdot\mathbf{u} = 0 \quad \text{in } \Omega,\ t>0, \tag{2}$$

$$\mathbf{u} = \mathbf{u}_{\partial\Omega} \quad \text{in } \partial\Omega,\ t>0, \tag{3}$$

$$\mathbf{u} = \mathbf{u}_0 \quad \text{in } \Omega,\ t=0, \tag{4}$$

where $\mathbf{b}$ is a volume force, $\mathbf{u}_{\partial\Omega}$ are the Dirichlet boundary conditions and $\mathbf{u}_0$ is the initial condition for the velocity field. Although, many phases can be present, we restrict here for the sake of simplicity to the case of two phase flows. Denoting them by the plus "+" and minus "-" symbols, the fluid properties (density and viscosity) are given by

$$(\rho(\mathbf{x}),\mu(\mathbf{x})) = \begin{cases} (\rho^+,\mu^+) & \text{if } \mathbf{x}\in\Omega^+ \\ (\rho^-,\mu^-) & \text{if } \mathbf{x}\in\Omega^- \end{cases} \tag{5}$$

The fluid domains $\Omega^+$ and $\Omega^-$ are separated by an interface denoted by $\Gamma$. In the following section we comment on the boundary or jump conditions at the this internal interface.



*Prepared using* fldauth.cls
DOI: 10.1002/fld

### 2.1. *Difficulties in the numerical solution of multi–phase flows - Jump conditions*

In the numerical approximation of incompressible multi–fluid flows several issues have to be considered

1. a correct definition of the interface position;
2. possible pressure gradient jumps or kinks at the interface where density jumps are present;
3. possible pressure jumps at the interface where viscosity jumps are present;
4. possible gradient velocity jumps where viscosity jumps are present;
5. possible pressure jumps where surface tension is present;

Some of these aspects and possible numerical solutions have been previously discussed in [9] for Lagrangian formulations in which moving meshes are used. In this paper we restrict our attention to items 2–5 of the list above for the case of Eulerian formulations in which fixed meshes are used instead. Let us now see how these jumps appear in the different cases mentioned.

*Pressure gradient jumps*

Density jumps introduce a kink in the pressure field at the interface. This can be easily seen in the example of two fluids with different densities at rest one on top of the other inside a closed cavity. The hydrostatic pressure gradient is discontinuous at the interface. Since in this case the solution corresponds to an identically zero velocity field, the pressure gradient is simply given by

$$\nabla p = \rho\, \mathbf{b},$$

if the density has a jump at the interface and the volume force is continuous, we have

$$[\![\nabla p]\!] = [\![\rho\, \mathbf{b}]\!] = [\![\rho]\!]\, \mathbf{b} = (\rho^+ - \rho^-)\, \mathbf{b}, \tag{6}$$

where $[\![\cdot]\!]$ represents the jump of any quantity at the interface. A similar situation can occur in the case of a discontinuous volume force. This could be the case of an electric force acting just on one of the fluids, having for instance distributed electrical charges. As mentioned above, a remedy for this problem is the enrichment proposed in [42], which is later recalled.

*Jump conditions for a Newtonian fluid*

The standard jump conditions at internal boundaries are briefly recalled here. In the first place, the velocity field at the interface $\mathbf{u}$ is decomposed into its normal and tangential parts as follows

$$\mathbf{u} = u_n \mathbf{n} + \mathbf{u}_s, \tag{7}$$

where $u_n = \mathbf{u} \cdot \mathbf{n}$. The interface forces must balance the sum of the forces exerted on $\Gamma$ from the "positive" side, plus those from the "negative" side. This is expressed as

$$(\sigma^- - \sigma^+) \cdot \mathbf{n} = \mathbf{f}_\Gamma. \tag{8}$$

Now, for the *normal component* of this jump we have

$$[(\sigma^- - \sigma^+) \cdot \mathbf{n}] \cdot \mathbf{n} = [\![\sigma_{nn}]\!] = [\![-p + 2\,\mu \frac{\partial u_n}{\partial n}]\!] = f_{\Gamma n}. \tag{9}$$

For the tangential component, we project the right hand side of equation (8) onto the tangent plane to the interface



DOI: 10.1002/fld

$$\Pi_\Gamma \left[(\sigma^- - \sigma^+)\cdot \mathbf{n}\right] = \left[\!\left[ \mu \left( \frac{\partial \mathbf{u}_s}{\partial n} + \nabla_\Gamma u_n - \mathbb{H}\cdot \mathbf{u}_s \right) \right]\!\right] = \\ = \left[\!\left[ \mu \frac{\partial \mathbf{u}_s}{\partial n} \right]\!\right] + [\![\mu]\!](\nabla_\Gamma u_n - \mathbb{H}\cdot u_s) = \mathbf{f}_\Gamma s, \tag{10}$$

where $\Pi_\Gamma$ is the projector operator, that for a given vector $\mathbf{w}$ is given by

$$\Pi_\Gamma \mathbf{w} = \mathbf{w}_s = \mathbf{w} - w_n \mathbf{n} = (\mathbb{I} - \mathbf{n}\otimes\mathbf{n})\,\mathbf{w}, \tag{11}$$

The symbol $\nabla_\Gamma$ is the surface gradient, which, for a function $f$ defined on $\Gamma$, is given as

$$\nabla_\Gamma f = \Pi_\Gamma \nabla \tilde{f}, \tag{12}$$

where $\tilde{f} \in \mathcal{C}^1$ is an extension out of $\Gamma$ of $f$. For vector functions, this is applied componentwise. Finally, $\mathbb{H}\ (= \nabla_s \mathbf{n})$ is a symmetric tensor called the second fundamental form. This tensor contains the geometrical information of the interface. In particular, its trace is the well known mean curvature $\kappa$.

**Remark:** In the general case, both the pressure and the velocity gradient can be discontinuous at the interface. However, for problems involving surface tension, in the absence of Marangoni or thermocapillary effects, the force $\mathbf{f}_\Gamma$ is normal to the interface and given by

$$\mathbf{f}_\Gamma = \gamma\,\kappa\,\mathbf{n}, \tag{13}$$

where $\gamma$ is the (constant) surface tension coefficient. If viscosities of both fluids are the same, just the pressure exhibits a jump. In the numerical solution of problem (1)–(4) with the jump conditions (6)–(10), regardless of the method used, be it finite elements or finite differences, special care has to be taken to accomodate the discontinuities in the fluid–dynamical variables near the interface. In this article we use a finite element method of which the variational formulation is presented below. In this case, the key issue relies in how to choose the approximation spaces for pressure and velocity.

### 2.2. *Variational formulations*

The variational formulation for the problem to be solved is

*Find* $(\mathbf{u}, p) \in V \times Q$ *such that*

$$\int_\Omega \rho\,(\partial_t \mathbf{u} + \mathbf{u}\cdot\nabla\mathbf{u})\cdot\mathbf{v}\,d\Omega + \int_\Omega 2\mu\, D\mathbf{u} : D\mathbf{v}\,d\Omega - \\ - \int_\Omega p\,\nabla\cdot\mathbf{v}\,d\Omega = \int_\Omega \mathbf{b}\cdot\mathbf{v}\,d\Omega + \mathbf{f}_\Gamma(\mathbf{v}) \tag{14}$$

$$\int_\Omega q\,\nabla\cdot\mathbf{u}\,d\Omega = 0 \tag{15}$$

$\forall (\mathbf{v}, q) \in V \times Q$. The term $\mathbf{f}_\Gamma(\mathbf{v})$ in equation (14) represents the contribution of a singular force concentrated at the inteface $\Gamma$. For the case of surface tension we use a Laplace–Beltrami formulation (see e.g. [43, 32, 38]), i.e.

$$\mathbf{f}_\Gamma(\mathbf{v}) = -\int_\Gamma \gamma(\mathbf{x})\,(\mathbb{I} - \mathbf{n}\otimes\mathbf{n}) : \nabla\mathbf{v}\,d\Gamma, \tag{16}$$



*Prepared using* fldauth.cls
DOI: 10.1002/fld

that accounts for both,surface tension and Marangoni effects.

We use a stabilized formulation based on the ASGS (Algebraic Subgrid Scale) method for discretization (see e.g. [44] and references therein) together with a trapezoidal rule for temporal discretization and a monolithic approach solving simultaneously for velocity and pressure using a Newton–Raphson iterative method. The discrete variational formulation of this problem then reads

*Find* $(\mathbf{u}_h^{n+1}, p_h^{n+1}) \in V_h \times Q_h$ *such that*

$$\mathcal{R}_{\mathbf{u}} = \int_\Omega \boldsymbol{\mathcal{G}}_{\mathbf{u}} \cdot \mathbf{v}_h \, d\Omega + \int_\Omega 2\mu \nabla^S \mathbf{u}_h^{n+1} : \nabla \mathbf{v}_h \, d\Omega - \int_\Omega p_h^{n+1} \nabla \cdot \mathbf{v}_h \, d\Omega + \mathbf{f}_{\Gamma_h}^{n+1}(\mathbf{v}_h) +$$

$$+ \sum_{K \in \mathcal{T}_h} \tau_K \int_{\Omega_K} (\boldsymbol{\mathcal{G}}_{\mathbf{u}} + \nabla p_h^{n+1}) \cdot \mathbf{u}_h^n \cdot \nabla \mathbf{v}_h + \sum_{K \in \mathcal{T}_h} \int_{\Omega_K} \delta_K \, \nabla \cdot \mathbf{u}_h^{n+1} \, \nabla \cdot \mathbf{v}_h \, d\Omega = 0 \qquad (17)$$

$$\mathcal{R}_p = \int_\Omega q_h \, \nabla \cdot \mathbf{u}_h^{n+1} \, d\Omega + \sum_{K \in \mathcal{T}_h} \int_{\Omega_K} \frac{\tau_K}{\rho} (\boldsymbol{\mathcal{G}}_{\mathbf{u}} + \nabla p_h^{n+1}) \cdot \nabla q_h \, d\Omega = 0 \qquad (18)$$

$\forall (\mathbf{v}_h, q_h) \in V_h \times Q_h$. In (17), the term $\boldsymbol{\mathcal{G}}_{\boldsymbol{u}}$ is given by

$$\boldsymbol{\mathcal{G}}_{\mathbf{u}} = \rho \left( \frac{\mathbf{u}_h^{n+1} - \mathbf{u}_h^n}{\Delta t} + \mathbf{u}_h^{n+1} \cdot \nabla \mathbf{u}_h^{n+1} - \boldsymbol{b}^{n+1} \right), \qquad (19)$$

with $\Delta t$ the time step and the stabilization parameters given by

$$\tau_K = c \left[ 4 \frac{\nu}{h^2} + 2 \frac{|\mathbf{u}_h|_\infty^n}{h} \right]^{-1}, \quad \delta_K = 2\,\mu + \rho\, |\mathbf{u}_h|_\infty^n \, h_K, \qquad (20)$$

where $c$ is a tuning parameter, that for the academic problems shown in section 4 is taken equal to 1, while for the 3D examples is taken equal to 0.1.

Many authors introduce a regularized form of the Dirac delta function for the computation of $\mathbf{f}_{\Gamma_h}^{n+1}(\mathbf{v}_h)$ in (17) as proposed in [29, 45], therefore, the surface force is approximated as a volume force more or less concentrated around $\Gamma$ depending on an adjustable regularization parameter. In our formulation, we *do not* use such regularizations and instead compute this term exactly, which precisely leads to sharp variations through the interface in the pressure field. Solving problem (17)–(18) accurately, requires the finite element spaces to be appropriately chosen, so as to accomodate discontinuities and/or kinks in the pressure and velocity fields. We first focus on how to improve the accuracy of the numerical approximation in several problems involving jumps in the pressure field, for which we introduce a *new* enrichment space.

## 3. NEW ENRICHMENT SPACE FOR DISCONTINUOUS PRESSURES

First, consider a finite element partition $\mathcal{T}_h$ of the domain $\Omega$ into simplices (triangles in the two dimensional case and tetrahedra in the three dimensional case) and denote each element in the partition as $\Omega_K$. The number of vertices per element is denoted by $n_p$ (equal to 3 for triangles and 4 for tetrahedra). The interface $\Gamma_h$ is composed of straight segments (in 2D) or planar facets (in 3D) and does not conform with the element edges. The element $\Omega_K$ can then be split into two subelements $\Omega_K^+$ and $\Omega_K^-$. We illustrate a typical element cut by $\Gamma_h$ in two and three spatial dimensions and the corresponding subdomains in figure 1. Those cases in which the interface passes through the nodes are degenerate cases that are not considered here. As noticed in figure 1 for the three dimensional case, two possible situations have to be considered, since the reconstructed interface can be either a triangular or a quadrangular facet. In the discrete variational formulation presented above, the integrals over the elements are performed exactly just by redefining the quadrature rule in the elements cut by the interface after subdivision following $\Gamma_h$. The velocity




DOI: 10.1002/fld

field is made up of continuous linear functions. For all the elements of $\mathcal{T}_h$ that are not crossed by $\Gamma_h$ the space $Q_h$ is also made up of continuous linear functions. *The various possibilities to improve accuracy of the numerical approximation in problems involving jumps or kinks, consist in an enrichment or a modification of the finite element space $Q_h$ only in those elements of $\mathcal{T}_h$ crossed by $\Gamma_h$.*

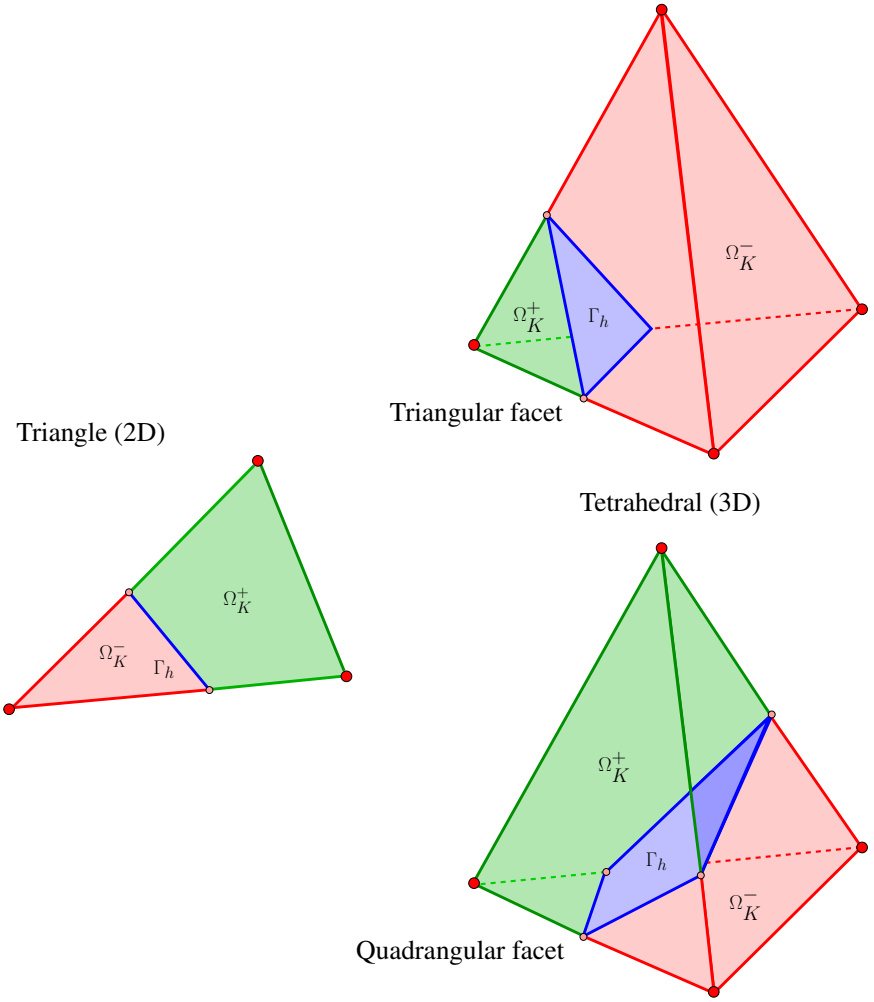


Figure 1. Typical element $\Omega_K$ and subelements $\Omega_K^+$ and $\Omega_K^-$ and interface $\Gamma_h$.

The discrete pressure proposed here can be written as

$$p_h = \sum_{J \in \mathcal{J}} P_J \, N_J + \sum_{J \in \mathcal{J}_e} C_J \, M_J, \tag{21}$$

where $\mathcal{J} = \{1, \ldots, n_P\}$, with $n_P$ the number of standard degrees of freedom per element and $\mathcal{J}_e$ the set of indices accounting for the additional enrichment functions local to the element.

In order to build the new pressure space, a requirement for the enrichment is that a constant solution on each fluid domain with a jump at the interface belong to the discrete space $Q_h$. To satify this requirement, we introduce two new enrichment functions that are linear on each subelement $\Omega_K^+$ and $\Omega_K^-$ and discontinuous at $\Gamma_h$. We also require both functions to be zero at the nodes of the simplex. By inspection, we see that a possibility to define the enrichment functions is as follows:



DOI: 10.1002/fld

$$M_1(\mathbf{x}) = (1 - S(\mathbf{x}))\,\chi^+(\mathbf{x}), \tag{22}$$
$$M_2(\mathbf{x}) = S(\mathbf{x})\,\chi^-(\mathbf{x}), \tag{23}$$

where the function $S$ is given in terms of the usual $P_1$ functions by

$$S = \sum_{J \in \mathcal{J}^+} N_J(\mathbf{x}), \tag{24}$$

with $\mathcal{J}^+ = \{J \in \mathcal{J},\, \mathbf{x}_J \in \Omega_K^+\}$, and $\chi^+$ and $\chi^-$ the characteristic functions for the positive and negative sides. The dimension of the pressure space is thus $\dim Q_h = N_P + 2\,N_E$, where $N_P$ and $N_E$ are the total number of nodes and elements respectively in $\mathcal{T}_h$. However, since, the additional shape functions are local to each element crossed by the interface, they can be condensed prior to assembly and the size of the final linear system to be solved is the same as in the standard case. Note that this elimination can be done because the pressure is just involved

In figure 2 the enrichment functions for a typical triangular element are shown. In the left part of the figure, the two functions are shown separately and in the right part they are plot together just for illustrative purposes. In table 2 the computation of these functions is given in the form of a pseudo–code.

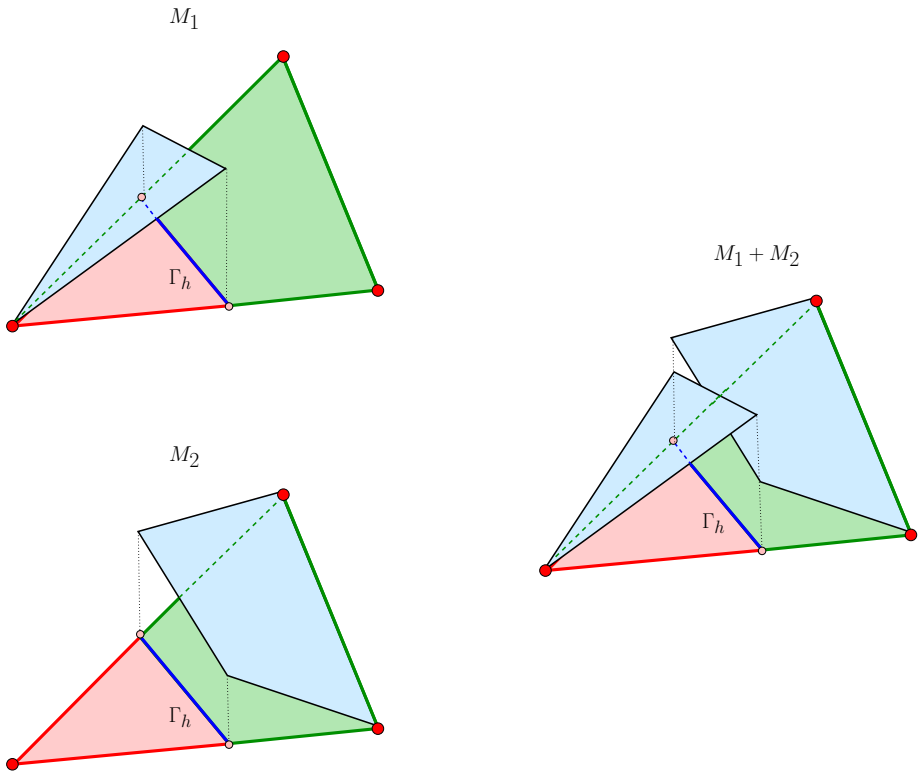


Figure 2. New enrichment functions in a typical triangular element. In the left, the two functions are drawn separately and in the right, the two functions are drawn together just for illustrative purposes.

### *3.1. Static elimination of the enrichment unknowns*

Before final assembly, the linear system to be solved at each non–linear iteration can be written by blocks as follows



DOI: 10.1002/fld

Table I. Computation of the new enrichment functions. Nomenclature: $n_p$ is the number of nodes per element, $n_G$ is the number of integration points per subelement, $N_I$ is the usual $I$–th linear basis function, $M_I$ $(I = 1, 2)$ are the new enrichment functions and $X_I^K$ are the vertices coordinates of element $\Omega_K$.

```
1: Subdivide element K in n_S subelements
2: do (s = 1, n_S)
3:  Set Gauss points x_j^s , for j = 1, ..., n_G
4:  do (i = 1, n_G)
5:   Set S(x_i^s) = 0
6:   do (J = 1, n_p)
7:    if (X_J^K ∈ Ω_K^+)
8:     Set S(x_i^s) ← S(x_i^s) + N_J(x_i^s)
9:    end if
10:  end do
11:  if (x_i^s ∈ Ω_K^+)
12:    Set M_1(x_i^s) = 1 − S(x_i^s)
13:    Set M_2(x_i^s) = 0
14:  else
15:    Set M_1(x_i^s) = 0
16:    Set M_2(x_i^s) = S(x_i^s)
17:  end if
18:  end do
19: end do
```

$$\begin{bmatrix} \mathsf{A}_{SS} & \mathsf{A}_{SM} \\ \mathsf{A}_{MS} & \mathsf{A}_{MM} \end{bmatrix} \begin{bmatrix} \delta \mathbf{X}_S \\ \mathbf{X}_M \end{bmatrix} = - \begin{bmatrix} \boldsymbol{\mathcal{R}}_S \\ \boldsymbol{\mathcal{F}}_M \end{bmatrix} \tag{25}$$

where the subindex $S$ refers to the velocity and standard pressure degrees of freedom and the subindex $M$ refers to the additional degrees of freedom. At the elementary level the dimension of matrix $\mathsf{A}_{SS}$ is $n_p^2 \times n_p^2$, of matrix $\mathsf{A}_{SM}$ is $n_p^2 \times 2$, of matrix $\mathsf{A}_{MS}$ is $2 \times n_p^2$ and of matrix $\mathsf{A}_{MM}$ is $2 \times 2$ and its $IJ$ entry is given by

$$\mathsf{A}_{MM}^{IJ} = \frac{\tau_K}{\rho} \int_{\Omega_K} \nabla M_I \cdot \nabla M_J \, d\Omega \tag{26}$$

which for our case is a positive definite diagonal matrix, since note that $M_1 = 0$ and $M_2 \neq 0$ in $\Omega_K^+$ and $M_1 \neq 0$ and $M_2 = 0$ in $\Omega_K^-$. For the additional degrees of freedom we do not compute the incremental values, but the unknown $\mathbf{X}_M$ since the pressure is just involved in the linear terms of the problem. Now, using the fact that the enrichment functions are local to each element, we eliminate $\mathbf{X}_M$ at the elementary level before final assembly as follows

$$\left[\mathsf{A}_{SS} - \mathsf{A}_{SM}(\mathsf{A}_{MM})^{-1}\mathsf{A}_{MS}\right] \delta \mathbf{X}_S = -\boldsymbol{\mathcal{R}}_S + \mathsf{A}_{SM}(\mathsf{A}_{MM})^{-1}\boldsymbol{\mathcal{F}}_M \tag{27}$$

The enrichment shape functions can be normalized to avoid round–off errors in the computation of $(\mathsf{A}_{MM})^{-1}$. The normalization factor can be defined simply by doing an order of magnitude estimation. Since, each entry of $\mathsf{A}_{MM}$ is the product of derivatives of two linear shape functions of order $\sim 1/h^2$, that are integrated over the element volume, which is of order $\sim h^d$ and the stabilization $\tau_K/\rho \sim h^2/\mu$ (considering the viscous dominated case for simplicity), the normalization factor can be chosen to be of order $h^d/\mu$ so as to end up with entries of order $1$ in matrix $\mathsf{A}_{MM}$.



DOI: 10.1002/fld

Numerical results using the new enrichment space will be compared with the classical $P_1$–conforming space and with the space presented in [33] which is recalled here for completness.

### 3.2. *Space of [33] for discontinous pressures without additional unknowns*

The interpolation properties of the space proposed in [33] have also been discussed in [34]. In this case no additional degrees of freedom are incorporated but the pressure shape functions are modified so as to capture discontinuities in the pressure field. The modifications are local and can be computed element–by–element. The modified functions are piecewise linear on each side and only discontinuous at the interface $\Gamma_h$. They form a nodal basis, in the sense that they take the value one at their corresponding node and zero at the other nodes. To define them, we simply "carry" the value at each node towards the intersection of any edge emanating from it with the interface. The shape functions for a typical triangular element are shown in figure 3, but again, the functions for the case of tetrahedral elements can be easily built as shown in the pseudo–code given in table II.

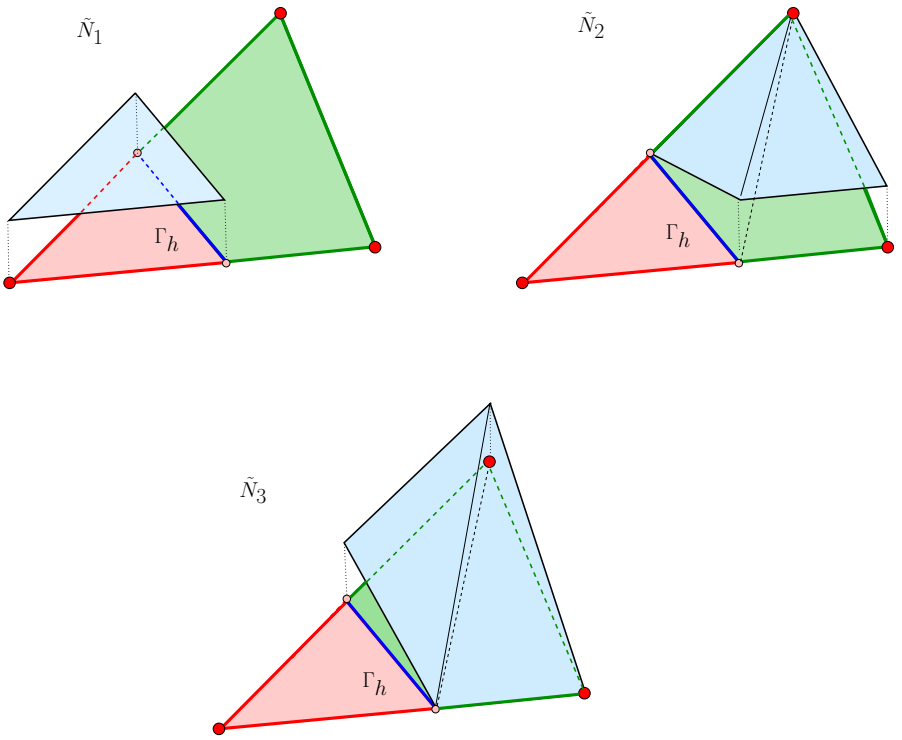


Figure 3. Finite element basis shape functions for the space proposed in [33] in a typical triangular element.

## 4. NUMERICAL TESTS

### 4.1. *Couette flow: Discontinuity in the pressure field due to a singular force*

In the first experiment, we consider the domain $[0, L] \times [0, H]$, with periodic boundary conditions in the $x_1$-direction. The velocity is set to zero at the top and bottom boundaries

$$\mathbf{u}(x_1, x_2 = 0) = \mathbf{u}(x_1, x_2 = H) = 0$$



DOI: 10.1002/fld

Table II. Computation of the basis functions for the space of [33]. Nomenclature: $n_p$ is the number of nodes per element, $n_G$ is the number of integration points per subelement, $N_I$ is the usual $I$–th linear basis function, $\tilde{N}_I$ $(I = 1, 2, 3)$ are the modified basis functions and $\boldsymbol{X}_I^K$ are the vertices coordinates of element $\Omega_K$.

```
1: Subdivide element K in n_S subelements
2: do (s = 1, n_S)
3:  Set subelement vertices X_J for J = 1, ..., n_p
4:  Set Gauss points x_j^s , for j = 1, ..., n_G
5:  do (i = 1, n_G)
6:   Set Ñ_I(x_i^s) = 0 for I = 1, ..., n_p
7:   do (I = 1, n_p)
8:    if ((X_I^K, x_i^s) ∈ Ω_K^+) || (X_I^K, x_i^s) ∈ Ω_K^-))
9:      do (J = 1, n_p)
10:       if (N_I(X_J^s) > 0) then
11:         Set Ñ_I(x_i^s) ← Ñ_I(x_i^s) + N_J(x_i^s)
12:       end if
13:     end do
14:   end if
15: end do
16: end do
```

and the interface $\Gamma$ is the straight vertical line $x_1 = a$, on which a constant unit normal force $f = 1$ is imposed. The exact solution for this problem is

$$u_1(x_1, x_2) = \frac{1}{2\mu L} x_2 (H - x_2) \tag{28}$$

$$u_2(x_1, x_2) = 0 \tag{29}$$

$$p(x_1, x_2) = -\frac{1}{L} x_1 + \mathcal{H}(x_1 - a) \tag{30}$$

The indeterminacy of the pressure is removed by imposing $p(0, 0) = 0$ instead of setting the average to zero, for simplicity. This problem, with $L = 3$, $H = 1$, $\mu = 1$ and $a = 2$ was discretized with the stabilized equal-order formulation presented above with the classical $P_1$-conforming pressure space, the space of [33] and the new enrichment space.

A sequence of unstructured meshes was built, of which the first one is shown in Fig. 4. To this mesh, which consists of 3520 triangles, we assign a mesh size of $h = 0.044$. The following meshes in the sequence are built by subdivision. We measure the velocity error in the $H^1(\Omega)$–norm and the pressure error in the $L^2(\Omega)$–norm as function of $h$ for both pressure spaces. The results of the convergence analysis are displayed in figures 5 and 6. As seen in the figures the error is very similar for both cases.

The pressure field corresponding to the classical $P_1$-conforming pressure is compared to that obtained using the new enrichment space in Fig. 7. From the figure we see that, the new enrichment space exhibits significantly better behavior near the interface than the classical $P_1$-conforming space. Results obtained using the space of [33] are similar to those corresponding to the new space.

### *4.2. Extensional flow: Discontinuity in the pressure field due to a jump in the viscosity*

We consider an extensional flow problem in which the computational domain $[0, 1] \times [0, 1]$ is split by an interface separating fluids with different viscosities $\mu_1$ and $\mu_2$. The density $\rho$ is assumed the same for both fluids. In this case, the interface $\Gamma$ is the straight horizontal line $x_2 = a$. Considering the following linear velocity field



DOI: 10.1002/fld

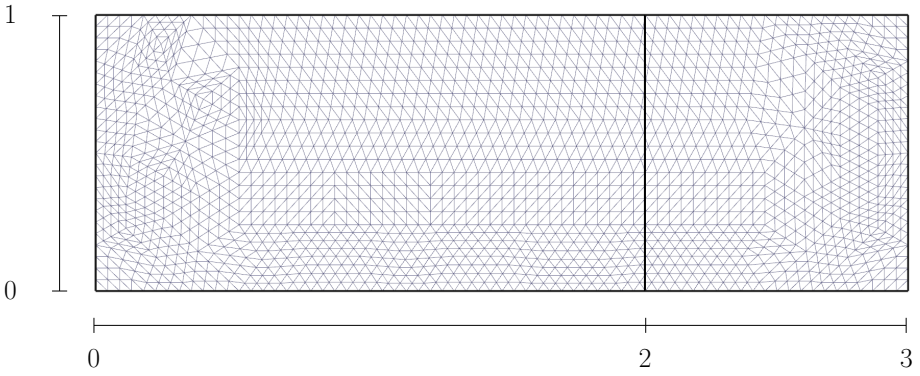


Figure 4. Mesh for the Couette flow problem convergence study, with 3520 elements and $h = 0.044$.

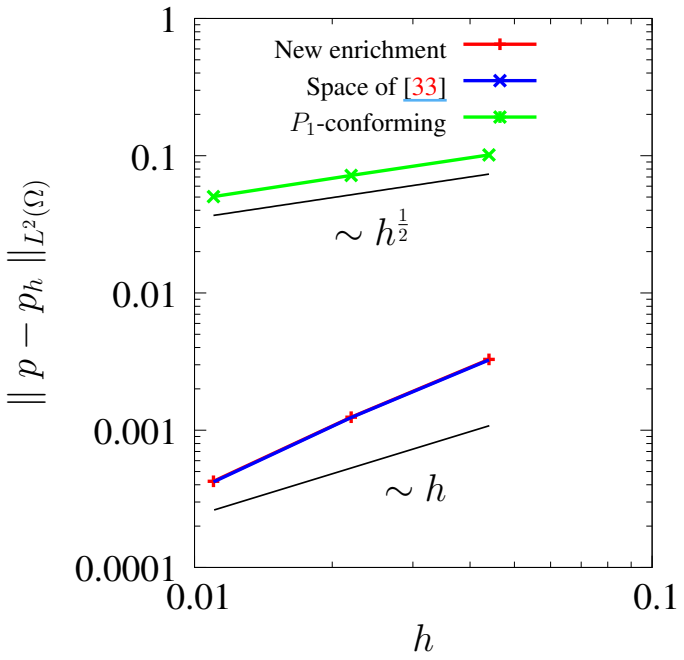


Figure 5. Error norm for the pressure field, showing the convergence rates for the Couette flow problem.

$$u_1(x_1, x_2) = 1 - x_1, \tag{31}$$
$$u_2(x_1, x_2) = x_2, \tag{32}$$

and neglecting the volume forces, it can be easily found that the exact solution for the pressure field is quadratic on each fluid and with a jump at the interface due to the viscosity difference. This pressure field is given by

$$p(x_1, x_2) = \rho \left( x_1 - \tfrac{1}{2}(x_1^2 + x_2^2) \right) + 2(\mu_1 - \mu_2)\mathcal{H}(a - x_2) \tag{33}$$

where $\mathcal{H}(a - x_2) = 1$ if $x_2 < a$ and zero otherwise. The indeterminacy of the pressure in the simulations is again removed by imposing $p(1, 1) = 0$ instead of setting the average to zero. In order to reproduce this exact solution, the velocity field given by (31)–(32) is imposed at the boundaries.



DOI: 10.1002/fld

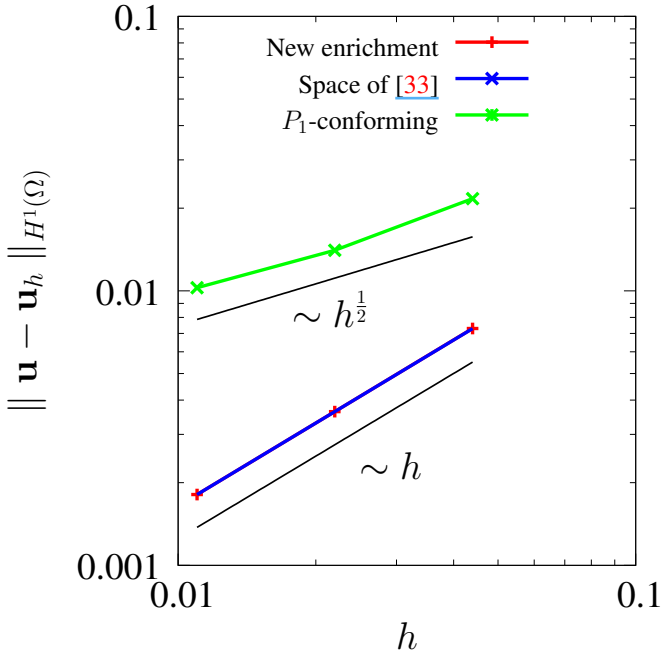


Figure 6. Error norm for the velocity field, showing the convergence rates for the Couette flow problem.

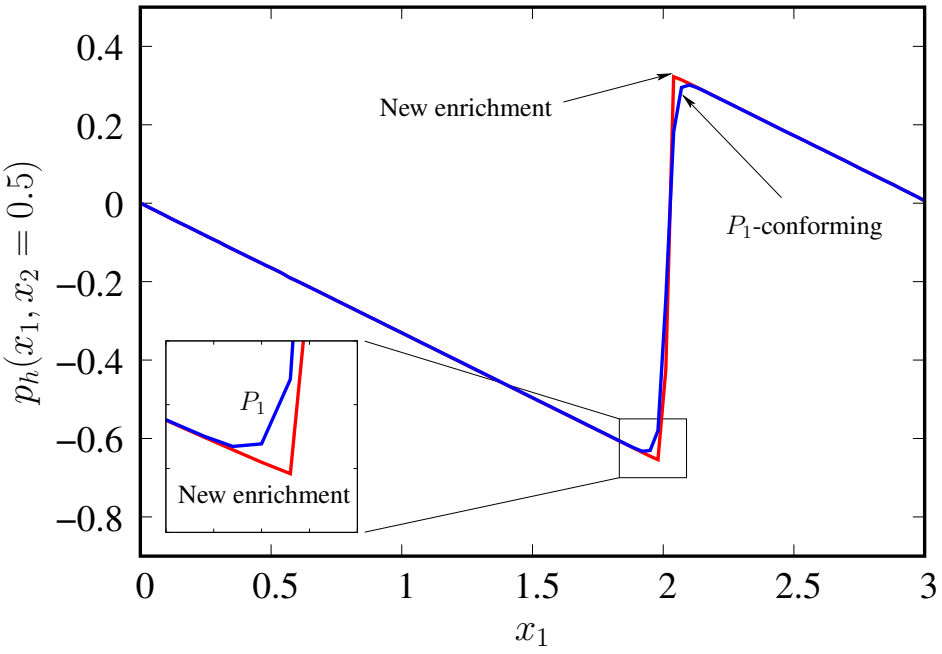


Figure 7. Pressure field section at $y = 0.5$ for the Couette flow problem.

The problem is solved with $\rho = 10$, $\mu_1 = 5$ and $\mu_2 = 1$ and $a = 0.5$ using the classical $P_1$-conforming pressure space, the new enrichment space and the space of [33]. A sequence of unstructured meshes was built, of which the first one is shown in Fig. 8. To this mesh, which consists of 1104 triangles, we assign a mesh size of $h = 0.0055$. The following meshes in the sequence are built by subdivision of each triangle into four equal triangles. We measure the velocity error in



DOI: 10.1002/fld

the $H^1(\Omega)$-norm and the pressure error in the $L^2(\Omega)$-norm as function of $h$. The results of the convergence analysis are displayed in Fig. 9 and 10. Results for the new enrichment space exhibit in this case a much smaller error (more than one order of magnitude) than results for the space of [33] in both pressure and velocity. Also, for the meshes considered, we observe a better convergence order of the new enrichment space, equal to $h^2$ for pressure and $h^{\frac{5}{2}}$ for velocity.

In Fig. 11 the pressure field for the the new enrichment space (left) and the classical $P_1$-conforming pressure space (right) are shown. In Fig. 12 cuts of these pressure fields at $x_1 = 0.5$ are compared, from which we clearly appreciate the better behavior near the interface when the new enrichment space is used. Note that the case without inertial effects (i.e. $\rho = 0$) corresponds to a constant pressure field on each fluid, with a jump at the interface of magnitude $2(\mu_1 - \mu_2)$. This solution belongs to the finite element spaces when either, the new enrichment space or the space of [33] are used.

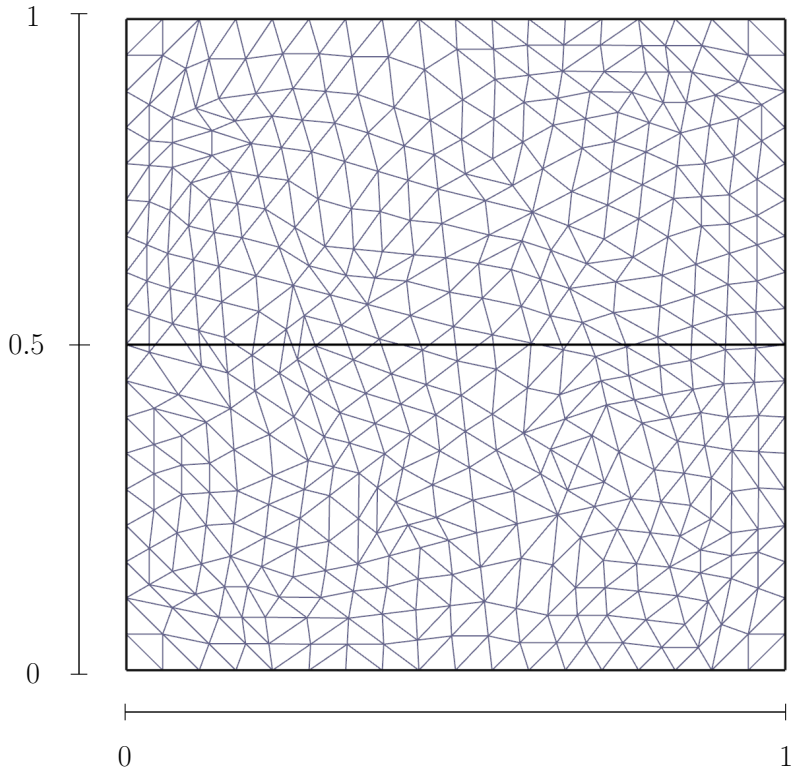


Figure 8. Mesh for the extensional flow problem convergence study, with 1104 elements and $h = 0.01$.

### *4.3. 3D Rising bubbles*

In the previous academic examples the interface $\Gamma$ was fixed. Now, we aim to show the good behavior of the new enrichment space in a more complex situation including the transport of the interface. In this article a level set formulation is used, in which the interface is the zero set of a continuous scalar function $\phi$, i.e.

$$\Gamma = \{\mathbf{x} \in \Omega,\ \phi(\mathbf{x}) = 0\}. \tag{34}$$

The level set function is transported according to the following hyperbolic equation

$$\partial_t \phi + \mathbf{u} \cdot \nabla \phi = 0. \tag{35}$$




DOI: 10.1002/fld

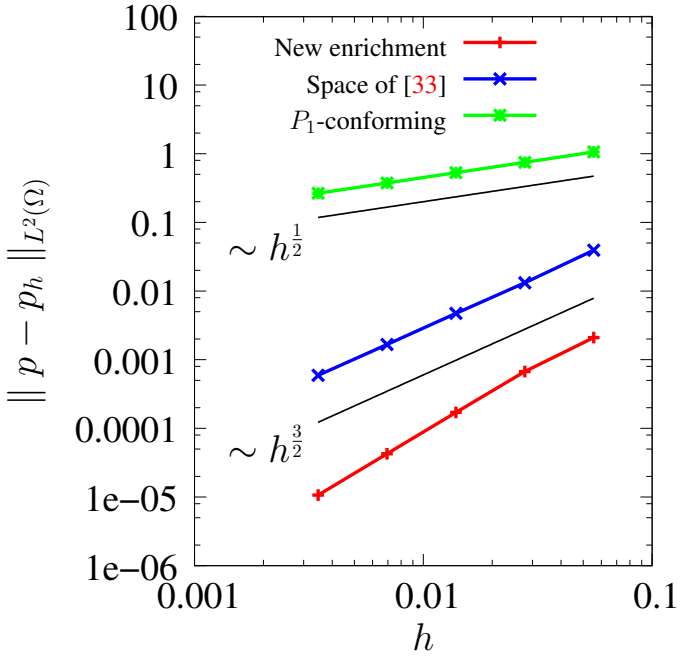


Figure 9. Error norm for the pressure field, showing the convergence rates for the extensional flow problem.

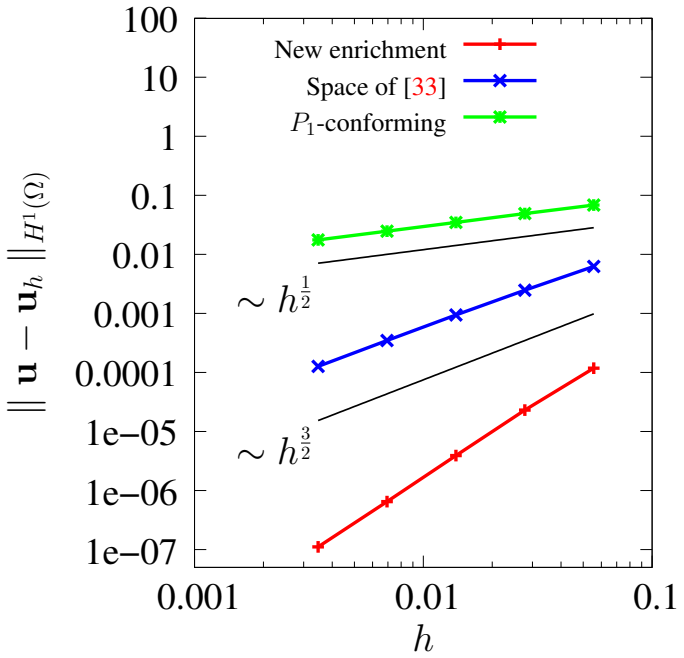


Figure 10. Error norm for the velocity, showing the convergence rates for the extensional flow problem.

In the discrete case, the transport equation is solved simultaneously with the velocity and pressure fields by means of a SUPG (streamline–upwind–Petrov–Galerkin) method (see [46]), by adding the following problem to the variational formulation (17)–(18)

*Find* $\phi_h^{n+1} \in W_h$ *such that*



DOI: 10.1002/fld

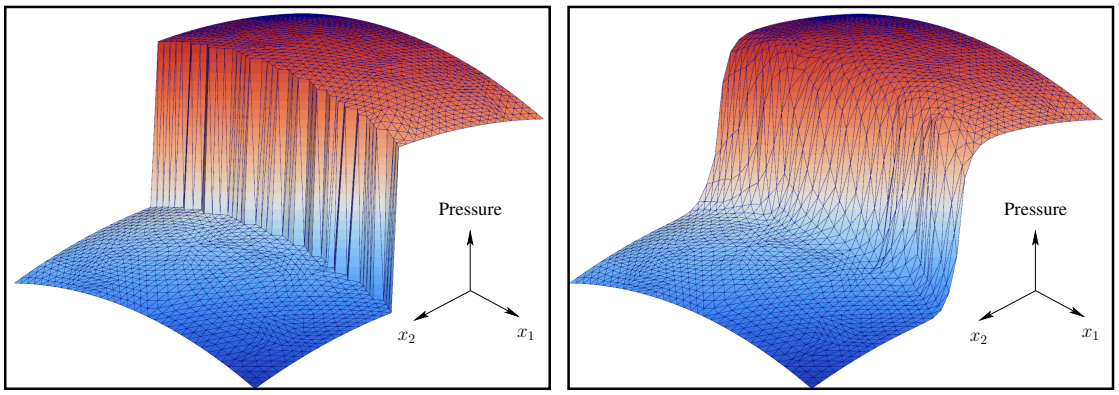


(a) New enrichment space

(b) $P_1$-conforming space

Figure 11. Pressure fields for the extensional flow problem. (a) New enrichment space. (b) $P_1$-conforming space.

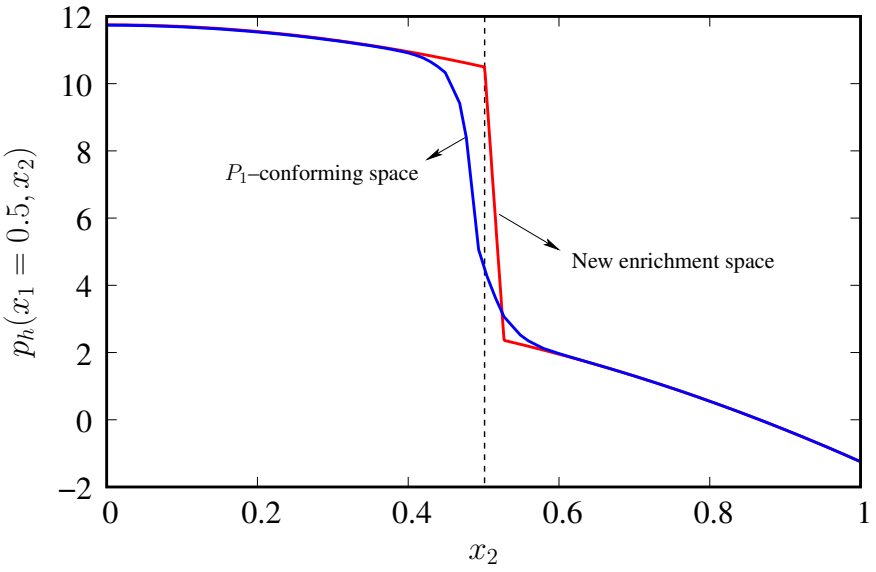


Figure 12. Comparison of the pressure field section at $x_1 = 0.5$ for the extensional flow problem using the the new enrichment space and the $P_1$-conforming space.

$$\sum_{K\in\mathcal{T}_h}\int_{\Omega_K}\left(\frac{\phi_h^{n+1}-\phi_h^n}{\Delta t}+\mathbf{u}_h^{n+1}\cdot\nabla\phi_h^{n+1}\right)\left(w_h+\tilde{\tau}_K\mathbf{u}_h^{n+1}\cdot\nabla w_h\right)d\Omega=0 \tag{36}$$

$\forall w_h \times W_h$. The discrete space $W_h$ is made up of continuous linear functions. The stabilization parameter $\tilde{\tau}_K$ is given by

$$\tilde{\tau}_K=\frac{\tilde{c}\,h}{2\,|\mathbf{u}_h|_\infty}, \tag{37}$$

where the tuning factor $\tilde{c}$ is taken equal to 0.1. With this formulation, we study the rise of a buoyant bubble. This problem has been solved many times before (see e.g. [47] and references therein). We assumme a bubble with density $\rho_1 = 10^{-3}$ and viscosity $\mu_1$ in a quiescent liquid with density $\rho_2 = 1$



DOI: 10.1002/fld

and viscosity $\mu_2$ in the computational domain $\Omega = (0, 2.25) \times (0, 2.25) \times (0, 4)$. At the initial time the diameter of the bubble is 1 and is placed at the position $(1.125, 1.125, 1)$. The gravity $g$ is taken to 10. We consider two different regimes corresponding to the following physical parameters

- Spherical regime: $\mu_1 = 3 \times 10^{-4}$, $\mu_2 = 0.3$, $\gamma = 10$
- Skirted regime: $\mu_1 = 10^{-3}$, $\mu_2 = 0.1$, $\gamma = 0.1$

In the first case, labeled spherical regime, the problem is dominated by surface tension effects and the bubble's shape remains approximatelly spherical during its evolution. In the second case, labeled skirted regime, surface tension effects are less important and the bubble suffers a larger deformation during the evolution.

The discrete variational formulation with the new enrichment space was included into a general purpose in–house code which is described elsewhere (see [48]). The level set function is periodically reinitialized by means of a mass–preserving redistancing scheme (see [49, 50]) to keep its distortion under control. For this problem, the finite element mesh used consists of $1,511,016$ tetrahedra and the time step is taken equal to $5 \times 10^{-4}$ for both regimes.

For the spherical regime, shown in figure 13 is the interface shape at times $t = 0$, $0.375$ and $0.75$. The bubbles are painted with the velocity magnitude. It is evident from the figure the benefits regarding mass conservation when the new enrichment space is used with respect to the classical $P_1$–conforming space. In the former case, a $2\%$ of the bubble's mass is lost at the final time shown in the figure against a $60\%$ in the case without enrichment.

For the skirted regime, to better appreciate the benefits of the new enrichment space, we plot in figure 14 the bubbles at different times together. We observe the typical cap shape attained by the bubble. For the case using the new enrichment, the bubble is plotted in the left side, in red, while for the case using the classical $P_1$-conforming space, the bubble is plotted in the right side, in blue. The mass lost is $\%0.14$ in the first case and $\%15$ in the second one, clearly evidencing the benefits of the new pressure space. For both regimes, similar results to those corresponding to the new enrichment are obtained if the space of [33] is used instead.

## 5. FURTHER ENRICHMENTS

We now discuss two further enrichments to improve accuracy of the numerical approximation in problems involving discontinuities and/or kinks. On the one hand, we propose to combine the enrichment function of Codina–Coppola [42] (for kinks in the pressure field) and the new enrichment functions proposed in this paper leading to a triple enrichment. We illustrate the triple enrichment by means of two numerical examples. On the other hand, we propose without testing it, an enrichment of the velocity field to capture discontinuities in its gradient. Its evaluation is the subject of ongoing work.

### *5.1. Enrichment space of Codina–Coppola for kinks in the pressure field*

For completness we recall here the enrichment proposed in [42]. In this case, one additional shape function local to the elements crossed by the interface is added. This function can be easily defined with the help of a level set function $\psi_h$ linearly interpolated on $\Omega_K$ and with the usual $P_1$ functions as follows

$$M_0(\mathbf{x}) = \frac{1}{2}\left(-|\psi_h(\mathbf{x})| + \sum_{J=1}^{n_p} |\psi_h(\mathbf{x}_J)| N_J(\mathbf{x})\right), \tag{38}$$

This function is zero outside $\Omega_K$ and can thus be condensed before assembly. The enrichment function is illustrated for a typical triangular element in figure 15 but the extension for the case of tetrahedral elements is straightforward as shown in table III where the code to calculate the shape function is included.



*Prepared using* fldauth.cls
DOI: 10.1002/fld

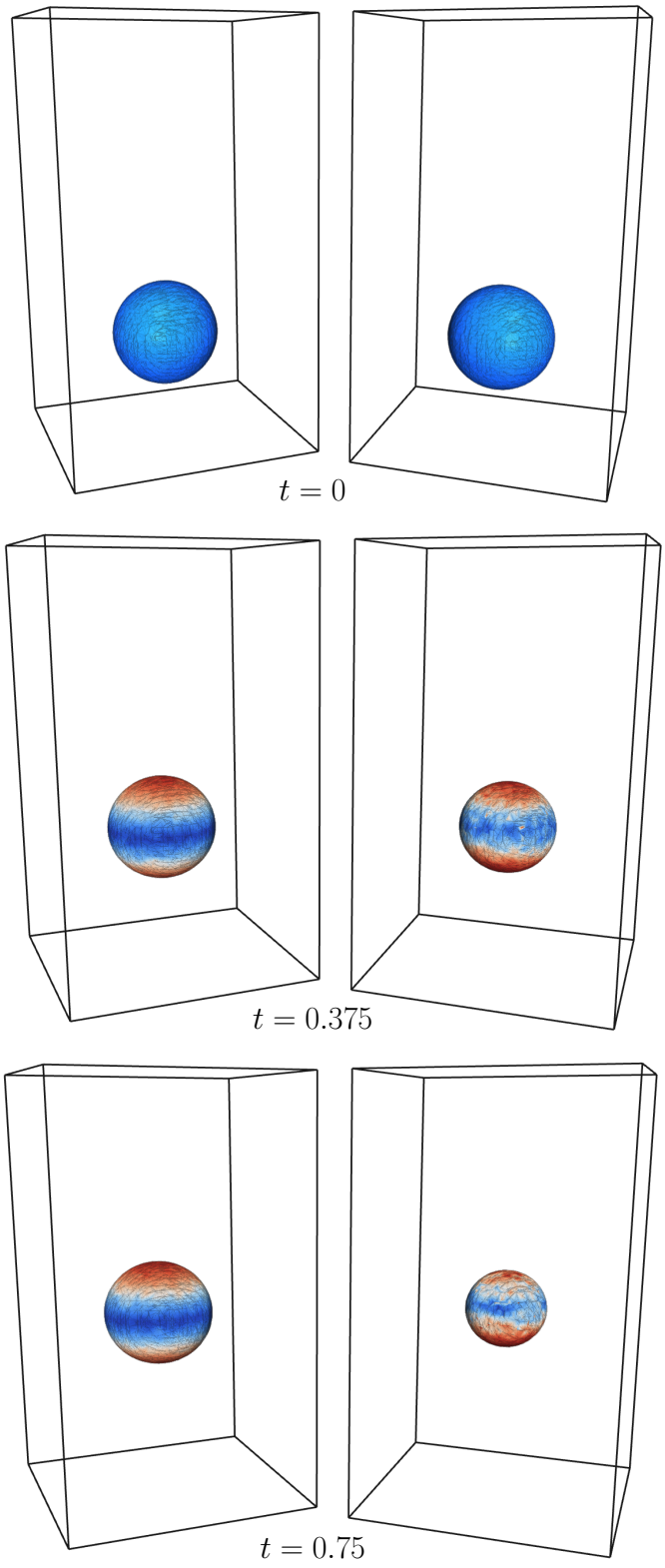


Figure 13. Comparison of the three dimensional rising bubble at different times for the spherical regime, using the new enrichment space (left) and the classical $P_1$-conforming space (right). For times $0.375$ and $0.75$, the maximum of the colour scale corresponds to $1.3$ (red) and the minimum to $0.02$ (blue).



DOI: 10.1002/fld

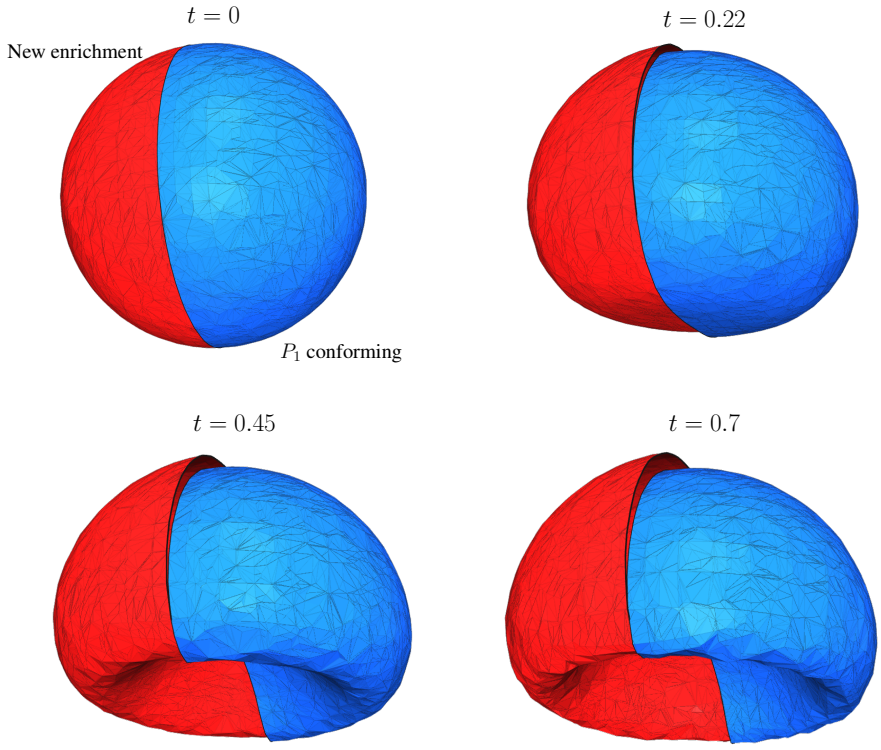


Figure 14. Comparison of the three dimensional rising bubbles at different times for the skirted regime, using the new enrichment space (left, red) and the classical $P_1$-conforming space (right, blue).

It is not difficult to see that the enrichment functions $M_0$, $M_1$ and $M_2$ are linearly dependent when the interface $\Gamma_h$ becomes parallel to one of the element faces. Although this is very unlikely to happen during a general dynamical calculation, the linear independence of the finite element basis may be deteriorated if the interface becomes nearly parallel to one of the faces, resulting in a $3 \times 3$ matrix $\mathsf{A}_{MM}$ in equation (25) approximately singular. This can be overcome by shifting the diagonal entries of $\mathsf{A}_{MM}$ by a small number when this situation is detected along a calculation, i.e.

$$\mathsf{A}_{MM} \leftarrow \mathsf{A}_{MM} + \varepsilon\, \mathsf{I}, \tag{39}$$

where $\mathsf{I}$ is the $3 \times 3$ identity matrix and $\varepsilon$ is a small parameter that for the problems presented in this paper we choose as $10^{-4} \sum_{I,J} |A^{IJ}_{MM}|$.

### 5.2. *Kinks and discontinuities in the pressure field*

*Two–fluid hydrostatic problem*

The prototypical example in which there is a discontinuity in the pressure field and its gradient is the case of a two–fluid hydrostatic problem. We consider two fluids in a unit square domain with densities $\rho_1$ and $\rho_2$ and separated by the fixed interface $x_2 = a$ (the lighter fluid on the top of the other). At the interface we introduce a singular force $f_\Gamma$ of size 100 as done in previous examples. The gravity $g$ is taken equal to $-10$, the viscosity $\mu$ equal to 1 for both fluids, $\rho_1 = 100$, $\rho_2 = 1$ and $a = 0.5$. Non–slip boundary conditions are used at all walls. The exact solution for this problem consists in a velocity field identically zero and a pressure field given by

$$p(x_1, x_2) = \begin{cases} \frac{1}{2}(\rho_1 - \rho_2)g + \rho_1\, g\, x_2 + f_\Gamma & \text{if } x_2 < a \\ \rho_2\, g(x_2 - 1) & \text{if } x_2 > a \end{cases} \tag{40}$$



DOI: 10.1002/fld

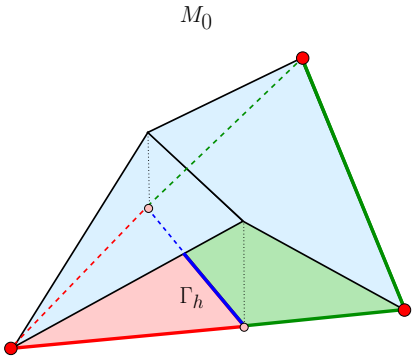


Figure 15. Codina-Owen's enrichment function proposed in [42] in a typical triangular element.

Table III. Computation of the enrichment function $N_0^e$ for the space of [42]. Nomenclature: $n_p$ is the number of nodes per element, $n_G$ is the number of integration points per subelement, $N_I$ is the usual $I$–th linear basis function, $M_0$ is the new enrichment function, $\boldsymbol{X}_I^K$ are the vertices coordinates of element $\Omega_K$ and $\psi_h$ is the linearly interpolated level set function on $\Omega_K$.

```
1: Subdivide element K in n_S subelements
2: do (s = 1, n_S)
3:  Set Gauss points x_j^s , for j = 1, ..., n_G
4:  do (i = 1, n_G)
5:    Set M_0(x_i^s) = 0
6:    if (ψ_h(x_i^s) > 0)
7:     Set M_0(x_i^s) = −ψ_h(x_i^s)
8:    end if
9:   do (J = 1, n_p)
10:    if (ψ_h(X_J^K) > 0) then
11:      Set M_0(x_i^s) ← M_0(x_i^s) + ψ_h(X_J^K) * N_J(x_i^s)
12:    end if
13:  end do
14: end do
15: end do
```

Note that, there is a discontinuity in the pressure field of size $f_\Gamma$ and a discontinuity in its gradient of size $(\rho_1 - \rho_2)g = 990$. In table IV we show the $L^2(\Omega)$ and the $H^1(\Omega)$ error norms for the pressure and the velocity fields respectively, for two different meshes with characteristic sizes $h = 0.0275$ and $h = 0.006875$ (the second and fourth meshes of the sequence used in problem 4.2) and using different finite element spaces. We consider, on the one hand, the combination of the enrichment of Codina–Coppola with the new enrichment space and the combination of the enrichment of Codina–Coppola with the space of [33]. In the first case, the error is almost zero since the exact solution simply belongs to the finite element space. In the second and third cases, the approximation error is significantly bigger since the exact solution is not in the approximation space.

*Extensional flow with discontinuous volume force*

We finally consider the same problem shown in section 4.2 but in this case we introduce a discontinuous volume force as follows

$$\mathbf{b} = \begin{cases} -10\,\mathbf{e}_2 & \text{if } x_2 < a \\ 0 & \text{if } x_2 > a \end{cases} \tag{41}$$



DOI: 10.1002/fld

Table IV. Error norms of pressure and velocity on two different meshes for the two–fluid hydrostatic problem.

| Pressure space | $h = 0.028$ | | $h = 0.007$ | |
|---|---|---|---|---|
| | $\|\mathbf{u} - \mathbf{u}_h\|_{H^1(\Omega)}$ | $\|p - p_h\|_{L^2(\Omega)}$ | $\|\mathbf{u} - \mathbf{u}_h\|_{H^1(\Omega)}$ | $\|p - p_h\|_{L^2(\Omega)}$ |
| New space + [42] | $10^{-13}$ | $10^{-13}$ | $10^{-13}$ | $10^{-13}$ |
| New space alone | 0.0206 | 0.1569 | 0.0023 | 0.0181 |
| Space of [33] + [42] | 0.1106 | 0.7574 | 0.0146 | 0.1018 |
| $P_1$ space alone | 8.0647 | 1.3995 | 3.9313 | 0.7456 |

As a result, the pressure field and its gradient are discontinuous, for which the triple enrichment used before becomes suitable. The pressure field for this problem is given by

$$p(x_1, x_2) = \rho \left( x_1 - \frac{1}{2}(x_1^2 + x_2^2) - |\mathbf{b}|\, x_2 \right) + 2(\mu_1 - \mu_2)\mathcal{H}(a - x_2) \tag{42}$$

in which there is a discontinuity of the pressure gradient of size $\rho\,|\mathbf{b}|$ and a discontinuity in the pressure of size $2\,(\mu_1 - \mu_2)$. In table V, we show the $L^2(\Omega)$–error norm for the pressure comparing the use of the new enrichment and the space of [33], both combined with the enrichment of [42]. Also shown in the table is the case corresponding to the new enrichment alone. The pressure field being a quadratic function, the exact solution does not belong to the finite element space. From the table we observe that the order of convergence for the pressure field is proportional to $h^2$ in the first case and proportional to $h^{3/2}$ in the second one. Besides this difference, again the new enrichment space exhibits significantly smaller errors.

Table V. $L^2(\Omega)$–error norm of the pressure as a function of the mesh size. Initial mesh with $h_0 = 0.056$.

| Pressure space | $h_0$ | $h_0/2$ | $h_0/4$ | $h_0/8$ | $h_0/16$ |
|---|---|---|---|---|---|
| New space + [42] | $1.73 \times 10^{-3}$ | $5.84 \times 10^{-4}$ | $1.44 \times 10^{-4}$ | $3.56 \times 10^{-5}$ | $8.91 \times 10^{-6}$ |
| New space alone | $5.98 \times 10^{-2}$ | $2.35 \times 10^{-2}$ | $7.95 \times 10^{-3}$ | $2.83 \times 10^{-3}$ | $1.02 \times 10^{-3}$ |
| Space of [33] + [42] | $2.55 \times 10^{-1}$ | $8.97 \times 10^{-2}$ | $3.31 \times 10^{-2}$ | $1.21 \times 10^{-2}$ | $4.21 \times 10^{-3}$ |

### *5.3. Kinks in the velocity field*

Although it has not been tested yet, using the enrichment functions proposed by Codina–Coppola, a new enrichment of the velocity field to capture kinks in the velocity field, for problems involving Marangoni effects or two phase flows with $\mu_1/\mu_2 \gg 1$ , can be devised. The idea in this case is to enrich each component of the velocity field as follows

$$u_i(\mathbf{x}) = \sum_{J \in \mathcal{J}} U_{iJ}\, N_J + \cos(\mathbf{n}, \mathbf{e}_i)\, U_e\, N_0^e. \tag{43}$$

The condensation of the new degree of freedom cannot be done in principle if we aim to ensure the conformity of the velocity field between contiguous elements, but, we consider that this can be done without introducing large errors, except perhaps in regions with high curvature, for which local mesh refinement may be needed. The evaluation of this enrichment is still the subject of ongoing work.

## 6. CONCLUSIONS

A new enrichment space have been proposed to accomodate discontinuities in the pressure field for problems involving jumps at internal interfaces in multi–fluid flows. The new space consist in



DOI: 10.1002/fld

adding two additional degrees of freedom that are local to each element and can thus be consended prior to assembly.

The new space has been tested and compared to other pressure spaces to accomodate discontinuities at immersed boundaries in several problems involving jumps in the pressure field and its gradient. In the classical Couette flow problem with a singular force the $L^2(\Omega)$ and $H^1(\Omega)$ error norms for pressure and velocity respectively, exhibited practically the same results as using the space of [33]. For the extensional flow problem, the error norms resulted in much smaller values (more than one order of magnitude) and with a better order of convergence for the new enrichment space as compared to the space of [33]. The new enrichment space has also been tested in a more challenging 3D problem involving a rising droplet in different regimes, exhibiting excelent results in terms of mass conservation as compared to the classical $P_1$–conforming space.

The possibility of combining the new enrichment with the enrichment proposed in [42] has also been explored in problems involving discontinuities and kinks in the pressure field due to the presence of singular forces and jumps in the density and/or in the volume forces. In this case, care that has to be taken to avoid lost of the linear independence of the finite element basis, which can occur when the interface becomes parallel to one of the element faces.

The new proposed enrichment space becomes then in a suitable alternative to other existing finite element spaces to accomodate jumps at immersed boundaries.

## REFERENCES


1. Sommerfeld M, van Wachem B, Oliemans R. Special interest group on dispersed turbulent multi–phase flow, best practice guidelines. *ERCOFTAC* 2007; .
2. Hughes T, Liu W, Zimmermann T. Lagrangian–Eulerian finite element formulation for incompressible viscous flows. *Comput. Meth. Appl. Mech. Engrg.* 1981; **29**:329–349.
3. Donea J, Huerta A, Ponthot JP, Rodríguez Ferran A. *Arbitrary Lagrangian-Eulerian methods*. Encyclopedia of Computational Mechanics, John Wiley & Sons, 2004.
4. Hirt C, Amsden A, Cook J. An Arbitrary–Lagrangian–Eulerian computing method for all flow speeds. *J. Comput. Phys.* 1974; **14**:227–253.
5. Cruchaga M, Calentano D, Tezduyar T. A moving Lagrangian interface technique for flow computations over fixed meshes. *Comput. Methods App. Mech. Engrg.* 2001; **191**:525–543.
6. Dettmer W, Saksono P, Perić D. On a finite element formulation for incompressible Newtonian fluid flows on moving domains in the presence of surface tension. *Commun. Numer. Meth. Engng.* 2003; **19**:659–668.
7. Baiges J, Codina R, Coppola-Owen H. The fixed-mesh ale approach for the numerical simulation of floating solids. *International Journal for Numerical Methods in Fluids* 2010; :n/a–n/adoi:10.1002/fld.2403. URL http://dx.doi.org/10.1002/fld.2403.
8. Idelsohn S, Oñate E, Del Pin F. The particle finite element method: A powerful tool to solve incompressible flows with free–surfaces and breaking waves. *Int. J. Num. Meth. Engrg.* 2004; **61**:964–989.
9. Idelsohn S, Mier-Torrecilla M, Oñate E. Multi–fluid flows with the particle finite element method. *Comput. Methods Appl. Mech. Engrg., In press* 2009; .
10. Unverdi S, Tryggvason G. A front–tracking method for viscous, incompressible, multi–fluid flows. *J. Comput. Phys.* 1992; **100**:25–37.
11. Gueyffier D, Lie J, Nadim A, Scardovelli R, Zaleski S. Volume–of–fluid interface tracking with smoothed surface stress methods for three–dimensional flows. *J. Comput. Phys.* 1999; **152**:423–456.
12. Popinet S, Zaleski S. A front-tracking algorithm for accurate representation of surface tension. *Int. J. Numer. Meth. Fluids* 1999; **30**:775–793.
13. Hirt C, Nichols H. Volume of fluid (VOF) methods for the dynamics of free boundaries. *Applied Numerical Mathematics* 1981; **39**:201–225.
14. Kothe D, Rider W, Mosso S, Brock J, Hochstein J. Volume tracking of interfaces having surface tension in two and three dimensions. *AIAA* 96-0859; .
15. Cummins S, Francois M, Kothe D. Estimating curvature from volume fraction. *Computers and Structures* 2005; **83**:425–434.
16. Adalsteinsson D, Sethian J. A fast level set method for propagating interfaces. *J. Comput. Phys.* 1995; **118**:269–277.
17. Sethian J. Evolution, implementation and application of level set and fast marching methods for advancing fronts. *J. Comput. Phys.* 2001; **169**:503–555.
18. Osher S, Fedkiw R. Level set methods: An overview and some recent results. *J. Comput. Phys.* 2001; **169**:463–502.
19. Guermond J, Quartapelle L. A projection FEM for variable density incompressible flows. *J. Comput. Phys.* 2000; **165**:167–188.
20. Shu C, Osher S. Efficient implementation of essentially non-oscillatory shock-capturing schemes. *J. Comput. Phys.* 1988; **77**:439–471.
21. Jiang GS, Peng D. Weighted ENO schemes for Hamilton-Jacobi equations. *SIAM J. Sci. Comput.* 2000; **21**:2126–2144.
22. Sweby P. High resolution schemes using flux limiters for hyperbolic conservation laws. *SIAM J. Numer. Anal.* 1984; **21**:995–1011.

23. Enright D, Fedkiw R, Ferziger J, Mitchell I. A hybrid particle level set method for improved interface capturing. *Computers and Structures* 2002; **83**:479–490.
24. Marchandise E, Remacle JF, Chevaugeon N. A quadrature-free discontinuous Galerkin method for the level set equation. *J. Comput. Phys.* 2006; **212**:338–357.
25. Di Pietro D, Lo Forte S, Parolini N. Mass preserving finite element implementations of the level set method. *Applied Numerical Mathematics* 2006; **56**:1179–1195.
26. Enright D, Losasso F, Fedkiw R. A fast and accurate semi-Lagrangian particle level set method. *Computers and Structures* 2005; **83**:479–490.
27. Strain J. Semi-Lagrangian methods for level set equations. *J. Comput. Phys.* 1999; **151**:498–533.
28. Strain J. Tree methods for moving interfaces. *J. Comput. Phys.* 1999; **151**:616–648.
29. Brackbill JU, Kothe DB, Zemach C. A continuum method for modeling surface tension. *J. Comput. Phys.* 1992; **100**:335–354.
30. Löhner R, Yang C, Oñate E. On the simulation of flows with violent free surface motion. *Comput. Methods Appl. Mech. Engrg.* 2006; **195**:5597–5620.
31. Carrica P, Wilson R, Stern F. An unsteady single–phase level set method for viscous free surface flows. *Int. J. Numer. Meth. Fluids* 2007; **53**:229–256.
32. Ganesan S, Matthies G, Tobiska L. On spurious velocities in incompressible flow problems with interfaces. *Comput. Methods Appl. Mech. Engrg.* 2007; **196**:1193–1202.
33. Ausas R, Sousa F, Buscaglia G. An improved finite element space for discontinuous pressures. *Comput. Methods Appl. Mech. Engrg.* 2010; **199**:1019–1031.
34. Buscaglia G, Agouzal A. Interpolation estimate for a finite element space with embedded discontinuities. *IMA Journal of Numerical Analysis, accepted* 2011; .
35. Minev PD, Chen T, Nandakumar K. A finite element technique for multifluid incompressible flow using Eulerian grids. *J. Comput. Phys.* 2003; **187**:255–273.
36. Chessa J, Belytschko T. A extended finite element method for two–phase fluids. *Journal of Applied Mechanics* 2003; **70**:10–17.
37. Belytschko T, Moës N, Usui S, Parimi C. Arbitrary discontinuities in finite elements. *Int. J. Numer. Meth. Engng* 2001; **50**:993–1013.
38. Gross S, Reusken A. Finite element discretization error analysis of a surface tension force in two-phase incompressible flows. *SIAM J. Numer. Anal.* 2007; **45**:1679–1700.
39. Gross S, Reusken A. An extended pressure finite element space for two-phase incompressible flows with surface tension. *J. Comput. Phys.* 2007; **224**:40–58.
40. Reusken A. Analysis of an extended pressure finite element space for two–phase incompressible flows. *Comput. Visual. Sci.* 2008; **11**:293–305.
41. Fries TP, Belytschko T. The intrinsic XFEM: a method for arbitrary discontinuities without additional unknowns. *Int. J. Numer. Meth. Engng.* 2006; **68**:1358–1385.
42. Coppola-Owen AH, Codina R. Improving eulerian two–phase flow finite element approximation with discontinuous gradient pressure shape functions. *Int. J. Numer. Meth. Fluids* 2005; **49**:1287–1304.
43. Bänsch E. Finite element discretization of the Navier–Stokes equation with a free capillary surface. *Numer. Math.* 2001; **88**:203–235.
44. Codina R. A stabilized finite element method for generalized stationary incompressible flows. *Comput. Methods Appl. Mech. Engrg.* 2001; **190**:2681–2706.
45. Chang Y, Hou T, Merriman B, Osher S. A level set formulation of eulerian capturing methods for incompressible fluid flows. *J. Comput. Phys.* 1996; **124**:449–464.
46. Hughes T. Recent progress in the development and understanding of SUPG methods with special reference to the compressible Euler and Navier–Stokes equations. *Int. J. Numer. Meth. Fluids* 1987; **7**:1261–1275.
47. Marchandise E, Geuzaine P, Chevaugeon N, Remacle JF. A stabilized finite element method using a discontinuous level set approach for the computation of bubble dynamics. *J. Comput. Phys.* 2007; **225**:949–974.
48. Ausas R. Numerical simulation in two–phase immiscible flows with applications in hydrodynamic lubrication. PhD Thesis, Engineering, Instituto Balseiro, April, 2010.
49. Mut F, Buscaglia G, Dari E. New mass-conserving algorithm for level set redistancing on unstructured meshes. *Journal of Applied Mechanics* 2006; **73**:1011–1016.
50. Ausas RF, Buscaglia GC, Dari EA. A geometric mass-preserving redistancing scheme for the level set function. *Int. J. Num. Meth. Fluids* 2010; **65**:989–1010.




DOI: 10.1002/fld